

Supplemental Material: Theory of potential impurity scattering in pressurized superconducting $\text{La}_3\text{Ni}_2\text{O}_7$

Steffen Bötzel,¹ Frank Lechermann,¹ Takasada Shibauchi,² and Ilya M. Eremin¹

¹*Institut für Theoretische Physik III, Ruhr-Universität Bochum, D-44780 Bochum, Germany*

²*Department of Advanced Materials Science, The University of Tokyo, Kashiwa, Chiba 277-8561, Japan*

Mixed solution and role of interorbital components for multiorbital La-327 model

In this section, additional information is given for the La-327 multiorbital model. We first consider the mixing of the interlayer gap component Δ_{\perp} with the intralayer component, *i.e.* extended s -wave component, Δ_s . In addition, we investigate the role of the interorbital components to the gap function and show how the gap function is renormalized in the disordered state in the process of the crossover from the s_{\pm} -wave to s_{++} -wave states, respectively.

In particular, in Fig. S1 we compare the effect of non-magnetic impurities for the simple bonding-antibonding (ba)- s_{\pm} -wave (magenta crosses) and the full s'_{\pm} wave solution $\Delta_{b/a} = \Delta_s \gamma_s \pm \Delta_{\perp}$ (red triangles) with $\gamma_{s/d} = (\cos(k_x) \pm \cos(k_y))/2$. The intralayer component Δ_s remains consistently significantly lower than Δ_{\perp} across all impurity densities considered, resulting in minimal impact on the shape of the T_c suppression curve. However, it is important to observe that the intralayer component exhibits a tendency to further mitigate the suppression of the unconventional s -wave superconductivity with increasing impurity density.

To elucidate the role of the hybridization between the $d_{x^2-y^2}$ and d_{z^2} orbitals we note that the $d_{x^2-y^2}$ -wave symmetric superconducting gap function with intraorbital gap $\Delta_{x^2-y^2}^{b/a}$ induces an interorbital gap $\Delta_{\text{inter}}^{b/a}$ of the form γ_d^2 . This can be seen by looking on the analytic form of the Green's function given in the Eq. (8) of the main text. Neglecting the impurity part, it reads

$$\hat{G}_{b/a}^{-1}(\mathbf{k}, i\omega_n) = i\omega_n \hat{1} - \hat{H}^{b/a}(\mathbf{k}) \hat{\tau}_3 - \hat{\Delta}^{b/a}(\mathbf{k}) \hat{\tau}_1, \quad (\text{S1})$$

where $\hat{\tau}_i$ denotes the i -th Pauli matrix in the Gor'kov-Nambu space. Starting with only $\Delta_{x^2-y^2}^{b/a} \neq 0$ and using the Cramer's rule, the interorbital anomalous component is given by

$$F_{\text{inter}}^{b/a}(\mathbf{k}, i\omega_n) = -V_{\mathbf{k}}^{b/a} \Delta_{x^2-y^2}^{b/a} (\epsilon_{z^2, \mathbf{k}}^{b/a} + i\omega_n) / \det(\hat{G}_{b/a}^{-1}(\mathbf{k}, i\omega_n)), \quad (\text{S2})$$

where $V_{\mathbf{k}}^{b/a}$ denotes the hybridization term and $\epsilon_{z^2, \mathbf{k}}^{b/a}$ denotes the intraorbital d_{z^2} component of $\hat{H}^{b/a}(\mathbf{k})$. Both, $V_{\mathbf{k}}^{b/a}$ and $\Delta_{x^2-y^2}^{b/a}$ contribute a form factor γ_d . Further, for dominant interlayer hopping, $\epsilon_{z^2, \mathbf{k}}^b$ and $\epsilon_{z^2, \mathbf{k}}^a$ will be of different

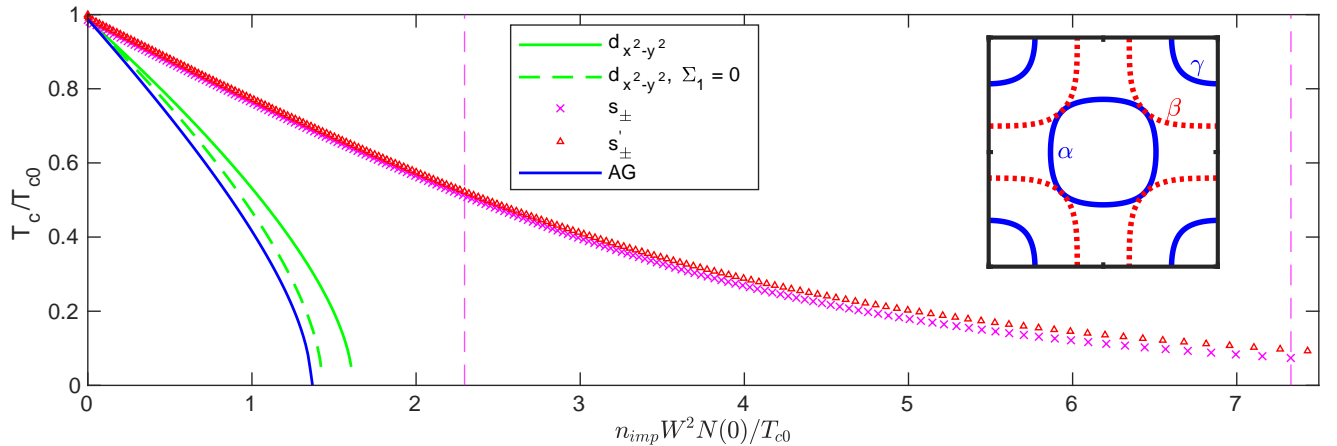


FIG. S1. (color online) Calculated T_c/T_{c0} suppression for the two-orbital bilayer $\text{La}_3\text{Ni}_2\text{O}_7$ model for the full s'_{\pm} wave solution $\Delta_{b/a} = \Delta_s \gamma_s \pm \Delta_{\perp}$ as compared to the pure interlayer s_{\pm} solution $\Delta_{b/a} = \pm \Delta_{\perp}$. We also plot the results for the in-plane $d_{x^2-y^2}$ -wave state, where the anomalous self energy is set to zero for simplicity. An Abrikosov-Gor'kov (AG) curve is shown for comparison. The vertical dashed lines denote the impurity densities for which the anomalous self-energy is plotted in Fig. S2(d-f) and Fig. S2(g-i).

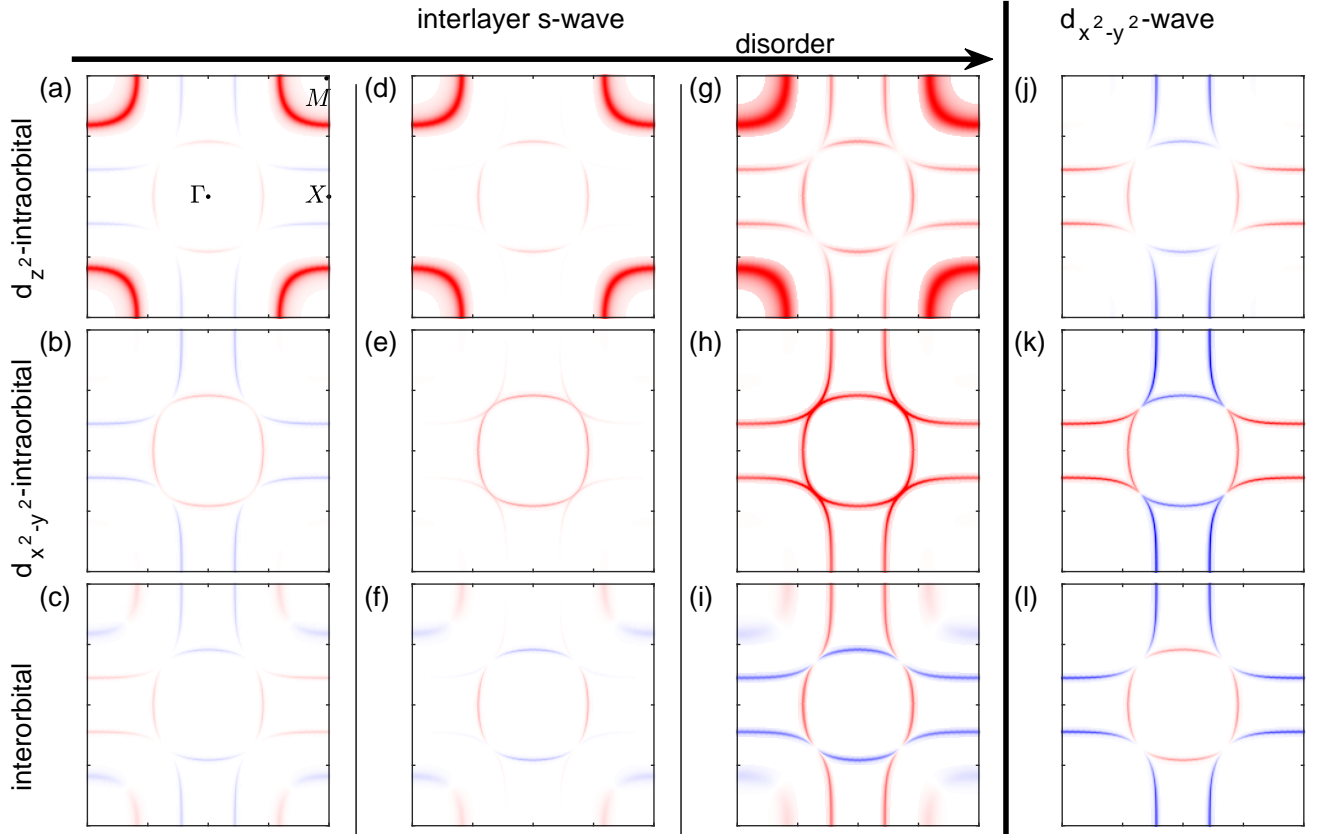


FIG. S2. (color online) Different orbital components of the anomalous Green's function in ba-space near T_c for various disorder levels. The first column (a)-(c) correspond to the ba- s_{\pm} -wave in the clean case. The second column (d)-(f) correspond to the ba- s -wave in the disordered state, as shown by the vertical dashed line in Fig.S1. The third column (g)-(i) visualizes the ba- s_{++} -wave after the s_{\pm} to s_{++} crossover already took place. The corresponding impurity densities for (d)-(f) and (g)-(i) are indicated by the vertical magenta dashed lines in Fig. S1). The fourth column shows the $d_{x^2-y^2}$ solution for the clean case, but the the structure does not qualitatively change upon adding disorder. Red and blue color scheme visualizes the sign and size of the superconducting gap function. The color scheme is fixed for each column but is different between different columns.

sign. Starting with only constant $\Delta_{z^2}^{b/a} \neq 0$, one similarly finds that $\Delta_{\text{inter}}^{b/a}$ follows γ_d due to hybridization and the overall s -wave symmetry is restored as the total contribution to the gap is proportional to γ_d^2 . We plot the real part of the different orbital components of the anomalous Green's function in ba-space for the lowest Matsubara frequency for the $d_{x^2-y^2}$ -wave and also the ba- s_{\pm} -wave in Fig. S2. This quantity is directly related to the superconducting gap function and importantly has the same symmetry in momentum space. Since we calculated near T_c , absolute values are small and only the relative values within each column (color scheme is only fixed within each column) are meaningful. In Fig. S2(a-c) and Fig. S2(j-l), the different orbital components are shown for the clean state for the ba- s_{\pm} and d -wave solutions. The interorbital components shown in the lowest row have a different symmetry as the intraorbital components as illustrated by the calculation above. For the ba- s_{\pm} the largest gap value is realized on the γ pocket, whereas it does not participate in the d -wave solution. This is expected because the γ pocket is of bonding- d_{z^2} character and the d -wave solution is in in-plane $d_{x^2-y^2}$ -orbital channel and the ba- s_{\pm} -wave is in the interlayer d_{z^2} -orbital channel. This also explains the absence of the intraorbital $d_{x^2-y^2}$ component on the γ pocket displayed in the second row.

We shall now incorporate disorder into the analysis. In Fig. S1, we compare T_c suppression curves for the $d_{x^2-y^2}$ -wave with and without neglecting the non-vanishing anomalous self-energy due to the interorbital component. The anomalous self-energy decreases the suppression rate slightly but without any qualitative change compared to Abrikosov-Gor'kov (AG) pair-breaking behavior. Since the interorbital component changes sign between bonding α and antibonding β band (Fig. S2(l)), this is exactly what is naively expected from the discussion of the ba- s -wave. However, it is in principle an interesting question whether this could be important in other systems. Although the suppression rate slightly decreases, the relative values of the different orbital components of superconducting gap do not significantly change compared to the clean case, presented in the fourth column in Fig. S2(j)-(l). As already

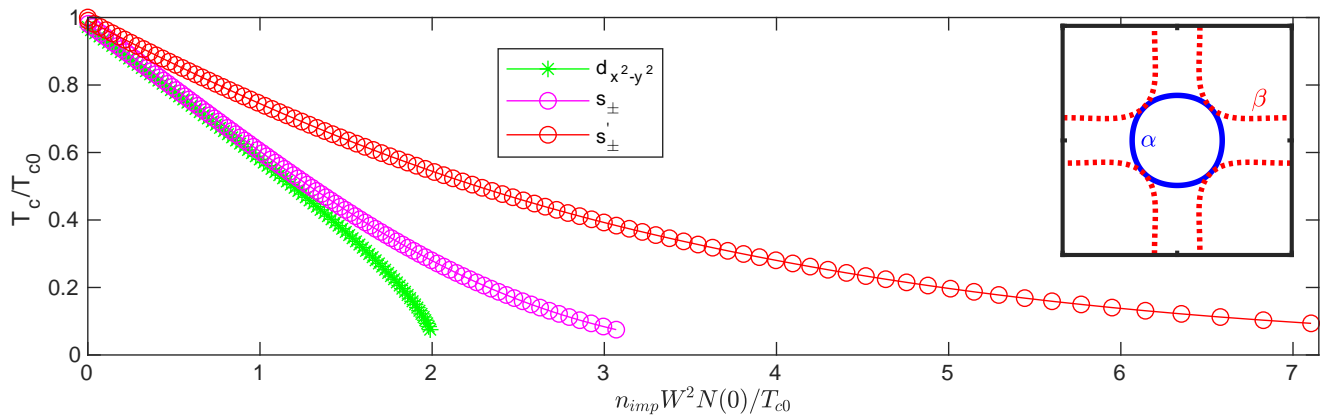


FIG. S3. (color online) T_c suppression for two-orbital bilayer $\text{La}_3\text{Ni}_2\text{O}_7$ model as in Fig.2(b) of the main text. Here, the full s'_{\pm} wave solution $\Delta_{b/a} = \Delta_s \gamma_s \pm \Delta_{\perp}$ is shown for comparison with the pure interlayer s_{\pm} solution $\Delta_{b/a} = \pm \Delta_{\perp}$. Here, the intra-layer component of the s'_{\pm} solution is dominant by an order of magnitude.

stated in the main text, the ba- s -wave solution displays a $s_{\pm} \rightarrow s_{++}$ crossover for the intraorbital components. This can be seen in the second and third columns of Fig. S2. The superconducting gap function on the antibonding band is suppressed more strongly than on the dominant bonding bands and vanishes at some points as can be seen in the second row Fig. S2(d)-(f). For higher disorder concentration, the superconducting gap function changes to s_{++} gap structure with the sign dictated by the dominant bonding subspace. Note that the amplitude of the gap function becomes more similar on the different orbital components and on different bands.

Mixed solution for multiorbital La-327 model and absence of γ pocket

In this section, the mixing of the interlayer gap component Δ_{\perp} with the extended intralayer component Δ_s is considered for the adapted multiorbital La-327 model, in which the γ band is pushed 50 meV below the Fermi level. In Fig. S3 the T_c suppression for two-orbital bilayer $\text{La}_3\text{Ni}_2\text{O}_7$ model from the main text (Fig. 2(b)) is compared to the mixed s' solution with $\Delta_{b/a} = \Delta_s \gamma_s \pm \Delta_{\perp}$ (red circles). For the mixed solution, we fix $J_{\perp}/J \approx 1.73$ to realistic values and adopt the interaction such that $T_c \approx 80$ K. In contrast to the case where the γ pocket is present on the Fermi surface, the intralayer Δ_s component becomes dominant, mediating a significant decrease in the suppression rate.

For comparison, we also investigated how the pure intralayer s -wave reacts to disorder in a single orbital case. By introducing $\Omega'_{b/a}$ implicitly via

$$\Sigma_1(\omega_n) = \frac{1}{2} n_{\text{imp}} W^2 \left[\tilde{\Delta}_b \sum_{\mathbf{k}} \frac{\gamma_s}{\tilde{\omega}_n^2 + \tilde{\epsilon}_{\mathbf{k},b}^2} + (b \leftrightarrow a) \right] =: \tilde{\Delta}_b \Omega'_b + \tilde{\Delta}_a \Omega'_a, \quad (\text{S3})$$

and we find the analogue to Eq. (18) of the main text. Inserting now $\Delta_{b/a} = \Delta_s \gamma_s$, the solution for $\tilde{\Delta}_{b/a}$ becomes

$$\tilde{\Delta}_{b/a} = \frac{\Delta_s \gamma_s}{1 - \Omega'_b - \Omega'_a}. \quad (\text{S4})$$

Without the γ_s form factor in the definition of $\Omega'_{b/a}$, this would together with $\tilde{\omega}_n = \omega_n / (1 - \Omega_b - \Omega_a)$ correspond to the expression from which the Anderson theorem can be derived [S1]. However, due to the γ_s form factor the suppression rate will depend on the details of the band structure.

Alternative single orbital model and fixed t_{\perp}

In this section, we repeat the calculation for another version of the single orbital model. To be precise, a momentum dependence to the interlayer hopping $t_{\perp} = t_{\perp,0} (\cos(k_x) - \cos(k_y))^2$ is added. The resulting band structure loosely

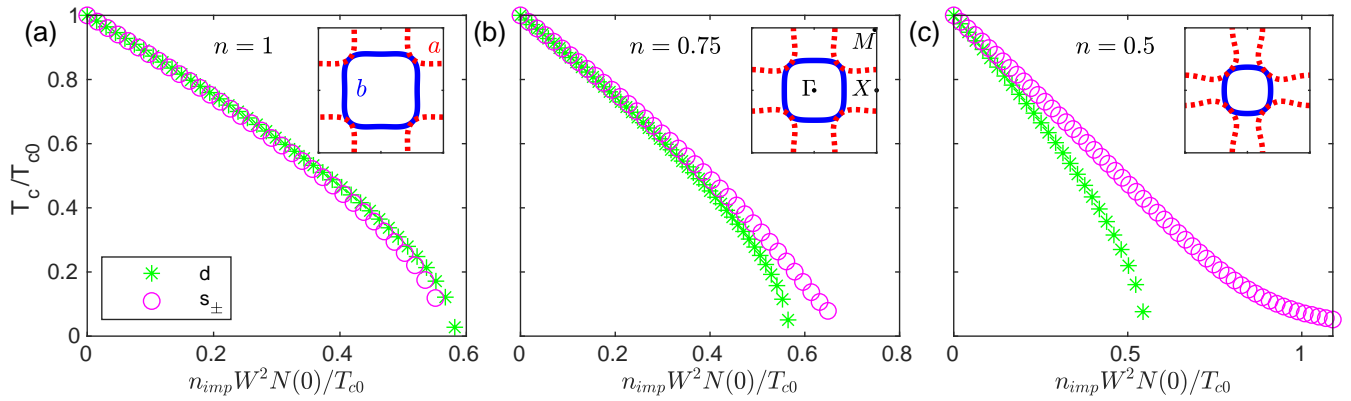


FIG. S4. (color online) T_c suppression for a single orbital bilayer model for $\Delta_{b/a} = \pm\Delta_{\perp}$ and $\Delta_{b/a} = \Delta_d\gamma_d$ for different fillings similar as for Fig.1 of the main text. Here, t_{\perp} is fixed and J and J_{\perp} are varied such that T_c is roughly the same for all cases.

resembles the α and β pockets for La-327 near quarter filling. Moreover, we maintain $t_{\perp,0} = t$ constant while exclusively varying J and J_{\perp} , in order to achieve an approximately equivalent T_c within the clean case. As in the main text, we consider half-filling $n = 1$, $n = 0.75$ and quarter filling $n = 0.5$. The corresponding T_c suppression curves are shown in Fig. S3. For the given momentum dependence $\epsilon_{\mathbf{k}}^b = -\epsilon_{\mathbf{k}+(\pi,\pi)}^a$ still holds at half-filling, which again ensures $\Omega_b = \Omega_a$ and consequently AG behavior at half-filling. The evolution of increasing imbalance between Ω_b and Ω_a decreasing the suppression rate is similar to the case considered in the main text. Let us for completeness mention, that the pure intralayer s -wave described in the previous section also becomes dominant at quarter filling (while vanishing for the other considered fillings) for both variations of the single orbital model.

Computational details

The Matsubara frequency cut-off for the summation over Matsubara frequencies is chosen as 16 eV. The quasiparticle energies and gap functions are discretized on a 100×100 k-mesh.

For the single orbital model, we self-consistently solve the linearized versions of Eq.(11)/(12) and Eqs.(14-16) of the main text and restrict ourselves to the pure interlayer ba - s_{\pm} -wave and d -wave case. In Fig. 1, we employ $t = 0.3$ and $J = 1.93t$, $t_{\perp} = 1.42t$ (a); $J = 1.6t$, $t_{\perp} = 1.54t$ (b) and $J = 1.1t$, $t_{\perp} = 1.78t$ (c). For Fig. S4, we used $t_{\perp} = t = 0.3$ and $J = 3t$, $J_{\perp} = 5t$ (a); $J = 2.67t$, $J_{\perp} = 4.67t$ (b) and $J = 2t$, $J_{\perp} = 4t$ (c). Studying the mixing of the ba - s_{\pm} -wave with a finite in-plane s -wave component, which is not shown, yields similar results as those in the multiorbital La-327 model. Alternatively, a finite ratio Δ_{\perp}/Δ_s in the $\Delta \rightarrow 0$ limit has to be allowed to vary freely in the full set of gap equations.

For the multiorbital La-327 model, we restricted the momentum summations to a 100 meV shell around the Fermi surface to reduce the numerical costs. To check the consistency, we applied this approximation to the single orbital model and verified that the suppression curves are minimally affected. We use $J = 2.36$ eV for the d -wave of the main text and $J_{\perp} = 1.93$ eV for the interlayer s -wave shown in Fig. 2(a) and Fig. S1. For the extended s -wave in Fig. S1, $J_{\perp} = 1.93$ eV and $J = (t/t_{\perp})^2 J \approx 1.73J$ are used. To shift the γ pocket 50 meV below the Fermi surface, we change the orbital on-site energy for the dz^2 -orbital from 0.459 eV to -0.095 eV. To achieve a fixed filling of 1.5, a chemical potential of $\mu \approx -0.307$ eV is necessary. For the interlayer ba - s -wave and d -wave shown in Fig. 2(b) and Fig. S3, $J_{\perp} = 6.4$ eV and $J = 2.4$ eV are used, respectively. For the intralayer dominated s -wave in Fig. S3, $J \approx 1.57$ eV and correspondingly $J_{\perp} = 2.71$ eV are used.

[S1] M. M. Korshunov, Y. N. Togushova, and O. V. Dolgov, Impurities in multiband superconductors, *Physics-Uspekhi* **59**, 1211–1240 (2016).